Laser catalysis with pulses

Amichay Vardi and Moshe Shapiro
Department of Chemical Physics, The Weizmann Institute of Science, Rehovot 76100, Israel
(Received 9 March 1998)

We present a time-dependent theory of laser catalysis, a process in which a strong light source is used to affect tunneling through a potential barrier by inducing a transient electronic excitation to a bound state. We have performed detailed calculations of pulsed laser catalysis on a one-dimensional Eckart potential as a function of the collision energy and the laser's central frequency. As in the cw case, the barrier transmission coefficients range from 100% tunneling on the blue side to complete suppression of tunneling on the red side of the radiatively broadened line. The point of perfect transmission is explained in the dressed state picture in terms of the equivalence between adiabatic laser catalysis and transmission through a double-barrier potential. The point of complete suppression of tunneling is shown to result from nonadiabatic destructive interference between the nonradiative tunneling and the optically assisted route. [S1050-2947(98)02708-5]

PACS number(s): 34.50.Rk, 42.50.Vk

I. INTRODUCTION

Over the past two decades a number of scenarios for laser acceleration and suppression of dissociation processes and chemical reactions have been proposed [1–21]. A theme common to many of these schemes is that lasers affect chemical reactivity by forming in conjunction with the molecule new (''dressed'') potentials. The dressed potentials may be more amenable to promoting a given reaction. The main difference between laser enhancement of chemical reactions and ordinary photochemistry is that the former is envisaged to involve no net absorption of laser photons. The concept of ''laser catalysis'' [14–16], i.e., a process in which a laser field after altering a reaction returns to its *exact* initial state, is a refinement of such scenarios.

Most of the past laser enhancement schemes require very high laser powers because the dressing of the potential surfaces [5,6,8] is ineffective due to the rather weak (collisionally or optically) induced nuclear dipole moments involved [9,11]. Thus, the use of ir radiation to overcome reaction barriers on the ground electronic surface [9,11] necessitates powers in the order of TW/cm^2. At these powers nonresonant multiphoton absorption, which invariably leads to ionization and/or dissociation, becomes dominant and drastically reduces the yield of the reaction of interest.

Free-free transitions involving excited electronic states [10] ought to require less power than those occurring on the ground state, because the laser in this case couples to strong electronic transition dipoles. However, even in this case the free-free nuclear factors reduce the transition-dipole matrix elements, and moreover, once the system is deposited on an unbounded excited electronic surface, it is impossible to prevent the reaction on that surface, and the resultant retention of the absorbed photon, from taking place. Such a chain of events resembles that of conventional (weak-field) photochemistry where the laser is used to impart energy to the reaction and not to catalyze it.

Scenarios [14–16] employing transitions between a scattering state on the ground electronic surface and a bound excited electronic state may ease the above power requirements, primarily because of the involvement of the much stronger bound-free nuclear factors. For an excited surface possessing no reaction barriers, such schemes give rise to ''laser catalysis'' [14–16], because the reagents, once excited, remain in the transition state region and shuttle freely between the reactants' side and the products' side of the ground-state barrier. If the energy available to the nuclei on the excited state is insufficient to break any bond, the system, not being able to escape the transition-state region, eventually relaxes (radiatively or nonradiatively) back to the ground state. In doing so, it has *a priori* similar probabilities of landing on the products' side as on the reactants' side of the barrier. If the laser is strong enough, the stimulated radiative relaxation route, yielding back the same photon absorbed, overcomes the nonradiative channels, resulting in true laser catalysis.

Detailed quantum-mechanical dressed-state computations of the cw laser catalysis of the symmetric $H+H_2 \rightarrow H_2+H$ reaction were performed [15,16]. These computations have shown that, whereas, as expected, the system relinquishes back the photon absorbed, if laser catalysis is performed with *coherent* light, the resulting molecular effect is not symmetric: The reaction probability follows a ''Fano-type'' [22] curve, in which the reaction probability is enhanced on the blue side of the absorption band and hindered on the red side. As a result, at a certain energy all the reagents end up on the products' side of the barrier, leading to a barrier transmission coefficient of unity, whereas at another energy tunneling is suppressed and the reaction probability is zero. The suppression of tunneling was interpreted as being due to destructive interference between nonradiative tunneling and the optical process.

Another scheme involving free-bound transitions to excited potential surfaces employs a two-pulse sequence [23,24]. According to this scenario, one can control exchange or bond breaking reactions on the ground potential surface by varying the delay between the excitation and deexcitation laser pulses. The lasers in such a two-pulse scheme do not act as catalysts since the first pulse is absorbed while the second pulse may be further strengthened, though not by the same amount.

The experimental implementations of laser catalysis were

hampered by the lack of calculations with *pulsed* sources. Though the cw calculations [15,16] have indicated that perfectly reasonable powers of hundreds of MW/cm^2 may be enough to bring about the desired effect, such powers can only be realized with pulsed lasers. The dressed-state methodology developed in Ref. [15] does not allow for the consideration of pulses and it was not known whether the effects noted for cw laser catalysis would be observed with pulses. In particular, because pulses are finite, it is *a priori* possible for some population to remain trapped in the excited bound state and never be deexcited down to the ground state.

Recently, we have developed an exact time-dependent formalism for treating dissociation [25–27] and recombination [28] due to the action of strong pulses. Both cases involve a bound manifold being coupled to a continuum by one or two laser pulses. In this paper (Sec. II) we extend this theory to the case of laser catalysis in which the strong laser pulse couples *two* continua (that of the reactants and that of the products) to a single bound manifold. In Sec. III we apply the theory to pulsed laser catalysis on a simple one-dimensional potential surface, for which analytic molecular eigenenergies and eigenfunctions are known. We present the evolution of the laser catalysis process with time and show that all the qualitative features of the cw case are obtained in the pulsed case, thus paving the way to the experimental realization of this process.

II. THEORY OF PULSED LASER CATALYSIS

We consider an $A+BC\rightarrow AB+C$ exchange reaction described by a smooth one-dimensional potential barrier along the reaction coordinate. The eigenstates of the system form a continuum of ''outgoing'' scattering states $|E,1^+\rangle$ and $|E,2^+\rangle$, with E being the total collision energy. The 1^+ and 2^+ indices are reminders that the reaction has originated in either arrangement channel 1, the $A+BC$ channel, or in channel 2, the $AB+C$ channel.

The asymptotic behavior of the $|E,1^+\rangle$ and $|E,2^+\rangle$ states is given by

$$\lim_{x\rightarrow-\infty}\langle x|E,1^+\rangle=\left(\frac{m}{k_1h}\right)^{1/2}\exp(ik_1x)+R_1(E)\exp(-ik_1x), \tag{1a}$$

$$\lim_{x\rightarrow+\infty}\langle x|E,1^+\rangle=T_1(E)\exp(ik_2x) \tag{1b}$$

and

$$\lim_{x\rightarrow\infty}\langle x|E,2^+\rangle=\left(\frac{m}{k_2h}\right)^{1/2}\exp(-ik_2x)+R_2(E)\exp(ik_2x), \tag{2a}$$

$$\lim_{x\rightarrow-\infty}\langle x|E,2^+\rangle=T_2(E)\exp(-ik_1x), \tag{2b}$$

where $k_{1,2}=\sqrt{2m[E-V(\mp\infty)]}/\hbar$.

The laser catalysis scenario is shown in Fig. 1: Under the action of a laser pulse of central frequency ω, assumed to be in near resonance with the transition from the continuum to an intermediate bound state $|0\rangle$, population is transferred

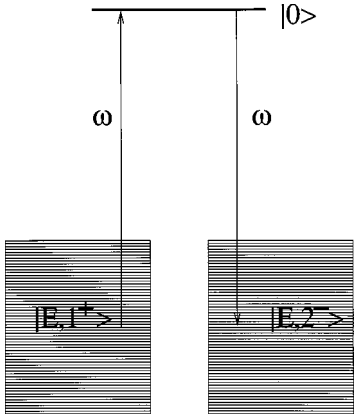

FIG. 1. Energy levels of the resonantly enhanced laser catalysis scheme.

from states $|E,1^+\rangle$ to a set of ''incoming'' scattering states $|E,2^-\rangle$, with the asymptotic behavior,

$$\lim_{x\rightarrow\infty}\langle x|E,2^-\rangle=\left(\frac{m}{k_2h}\right)^{1/2}\exp(ik_2x)+R_2^*(E)\exp(-ik_2x), \tag{3a}$$

$$\lim_{x\rightarrow-\infty}\langle x|E,2^-\rangle=T_2^*(E)\exp(ik_1x). \tag{3b}$$

Writing the total Hamiltonian of the system as

$$H_{\rm tot}=H-2\vec{\mu}\cdot\hat{\epsilon}\epsilon(t)\cos(\omega t), \tag{4}$$

where H is the radiation-free Hamiltonian, $\epsilon(t)$ is a ''slowly varying'' electric field amplitude, and $\vec{\mu}$ is an (electronic) transition dipole operator, we solve the dynamics embodied in the time-dependent Schrödinger equation

$$i\hbar\partial|\Psi\rangle/\partial t=H_{\rm tot}|\Psi\rangle, \tag{5}$$

by expanding the material wave function $|\Psi\rangle$ as

$$|\Psi(t)\rangle=b_0|0\rangle\exp(-iE_0t/\hbar)+\int dE[b_{E,1}(t)|E,1^+\rangle+b_{E,2}(t)|E,2^+\rangle]\exp(-iEt/\hbar), \tag{6}$$

where

$$[E_0-H]|0\rangle=[E-H]|E,n^+\rangle=0,\quad n=1,2. \tag{7}$$

Substitution of the expansion of Eq. (6) into the time-dependent Schrödinger equation, and use of the orthogonality of the $|0\rangle$, $|E,1^+\rangle$, and $|E,2^+\rangle$ basis states, results in an (indenumerable) set of first-order differential equations for the expansion coefficients. In the rotating-wave approximation, this set of equations is of the form

$$\frac{db_0}{dt}=i\int dE\sum_{n=1,2}\Omega_{0,E,n}(t)\exp(i\Delta_Et)b_{E,n}(t), \tag{8}$$

$$\frac{db_{E,m}}{dt}=i\Omega_{0,E,m}^*(t)\exp(-i\Delta_Et)b_0(t),\quad m=1,2, \tag{9}$$

where

$$\Omega_{0,E,n}(t) \equiv \langle 0|\mu|E,n^+\rangle \epsilon(t)/\hbar, \quad n=1,2 \tag{10}$$

and

$$\Delta_E \equiv (E_0 - E)/\hbar - \omega. \tag{11}$$

Substituting the formal solutions of Eq. (9),

$$b_{E,n}(t) = b_{E,n}(t_0) + i\int_{t_0}^{t} dt' \Omega^*_{0,E,n}(t') \exp(-i\Delta_E t') b_0(t'), \tag{12}$$

into Eq. (8), we obtain

$$\frac{db_0}{dt} = i\sum_{n=1,2}\int dE\ \Omega_{0,E,n}(t)\exp(i\Delta_E t) b_{E,n}(t=0) - \sum_{n=1,2}\int dE \int_{t_0}^{t} dt' \Omega_{0,E,n}(t)\Omega^*_{0,E,n}(t') \times \exp[(i\Delta_E(t-t')] b_0(t'). \tag{13}$$

If both molecular continua are unstructured, we can invoke the slowly varying continuum approximation (SVCA) [25–28]. In this approximation we replace the energy-dependent bound-free dipole-matrix elements at energies spanning the laser profile by their value at the pulse center, given (in the Λ configuration of Fig. 1) as $E_L = E_2 - \hbar\omega$,

$$|\langle 0|\mu|E,1^+\rangle|^2 + |\langle 0|\mu|E,2^+\rangle|^2 \approx |\langle 0|\mu|E_L,1^+\rangle|^2 + |\langle 0|\mu|E_L,2^+\rangle|^2. \tag{14}$$

The use of the SVCA greatly simplifies the equations because upon substitution of Eqs. (10) and (14) into Eq. (13) we can perform the integration over E and t' analytically. We obtain that

$$\frac{db_0}{dt} = \sum_{n=1,2} iF_n(t) - \Omega_n(t) b_0(t), \tag{15}$$

where

$$\Omega_n(t) \equiv \pi |\langle 0|\mu|E_L,n^+\rangle \epsilon(t)|^2/\hbar, \quad n=1,2. \tag{16}$$

The source terms $F_n(t)$ are given as

$$F_n(t) = \epsilon(t)\overline{\mu}_n(t)/\hbar, \quad n=1,2, \tag{17}$$

where

$$\overline{\mu}_n(t) = \int dE \langle 0|\mu|E,n^+\rangle \exp(i\Delta_E t) b_{E,n}(t_0), \quad n=1,2.$$

We can obtain analytical solutions of Eq. (15) in the form

$$b_0(t) = v(t)\phi(t) + b_0(t_0)v(t), \tag{18}$$

where

$$v(t) = \exp\left(-\int_{t_0}^{t}[\Omega_1(t') + \Omega_2(t')]dt'\right) \tag{19}$$

and

$$\phi(t) = i\int_{t_0}^{t} \frac{F_1(t') + F_2(t')}{v(t')}\, dt'. \tag{20}$$

In the laser-catalysis process, the initial conditions are such that $b_0(t_0) = 0$ and $b_{E,2}(t_0) = 0$ for all E. Therefore, we obtain for the $b_0(t)$ coefficient,

$$b_0(t) = i\int_{t_0}^{t} F_1(t')\exp\left(-\int_{t'}^{t}[\Omega_1(t'') + \Omega_2(t'')]dt''\right) dt'. \tag{21}$$

Given $b_0(t)$, the continuum population distributions $b_{E,1}(t)$ and $b_{E,2}(t)$ are obtained directly via Eq. (12). Typical potentials and eigenfunctions used to simulate one-photon laser catalysis are plotted in Fig. 2.

III. PULSED LASER CATALYSIS WITH A PAIR OF ECKART POTENTIALS

As a first application of the formalism of Sec. II we consider laser catalysis with an Eckart potential [29,30],

$$V_{\text{ground}}(x) = V[\xi(x)] = -\frac{A\xi}{1-\xi} - \frac{B\xi}{(1-\xi)^2}, \qquad \xi = -\exp(2\pi x/l) \tag{22}$$

for the ground state and an inverted Eckart potential,

$$V_{\text{excited}}(x) = \mathcal{E} - V[\xi(x)] \tag{23}$$

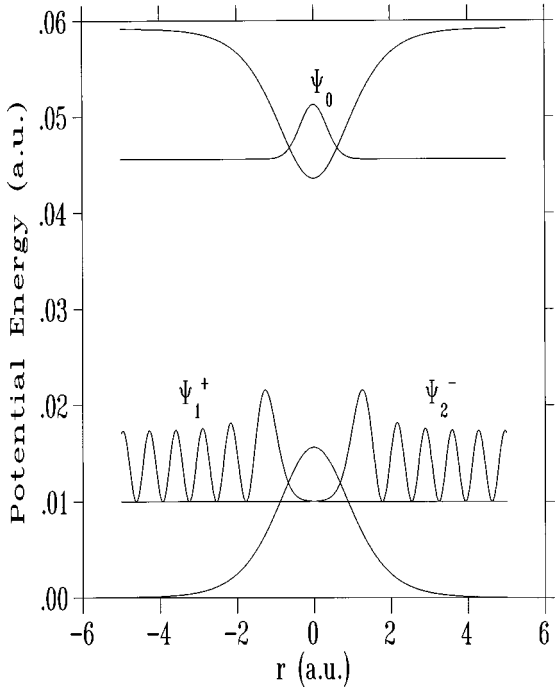

FIG. 2. Eckart potentials and wave functions used in the simulation of the laser catalysis process. Potential parameters were $A = 0$ a.u., $B = 6.247$ a.u., $l = 4.0$ a.u., and $m = 1060.83$ a.u.

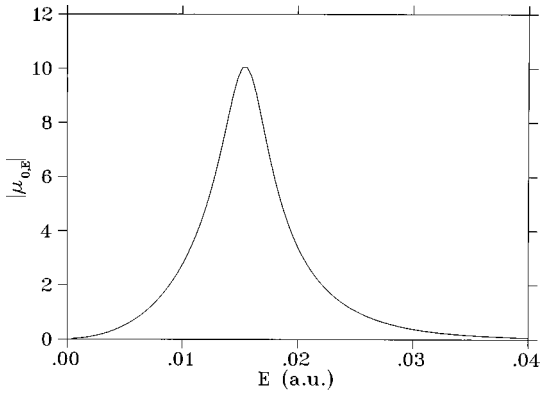

FIG. 3. Free-bound transition matrix elements vs collision energy.

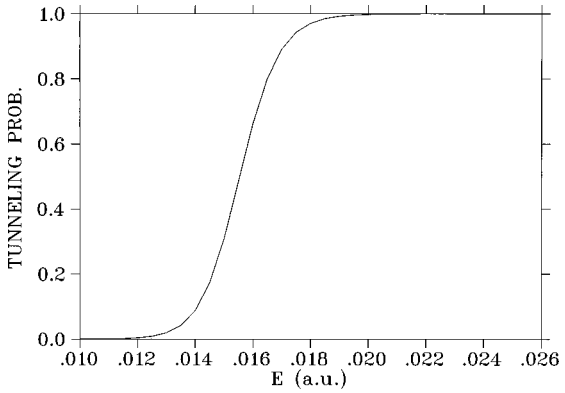

FIG. 4. Nonradiative reactive probability as a function of collision energy.

having a well for the excited state. The asymptotic values for the Eckart potential are

$$V(x=-\infty)=0, \quad V(x=+\infty)=A \tag{24}$$

and the barrier height is given as

$$V_{\max}=\frac{(A+B)^2}{4B}. \tag{25}$$

The Schrödinger equation with the Eckart potential has well known analytical solutions for both bound and continuum $|E,n^+\rangle$ states [29,30]. Theses solutions are spelled out in detail in the Appendix, where some errors that have persisted in the literature have been corrected. The parameters of Eq. (22) chosen for the ground Eckart potential are $A=0$, $B=6.247\times10^{-2}$ a.u., and $l=40$ a.u. The particle's mass m was chosen as that of the $H+H_2\rightarrow H_2+H$ reaction, i.e., $m=1060.83$ a.u. The intermediate state was the $v=0$ level of the inverse Eckart potential given in Eq. (23), with the same parameters. Potential parameters were chosen to resemble the energy profile along the reaction path for the linear $H+H_2\rightarrow H_2+H$ reaction [31,32]. The resulting potential curves are plotted in Fig. 2. Given these parameters, eigenfunctions and eigenenergies were obtained using the formulas of the Appendix, and the bound-continuum dipole matrix elements $\langle 0|\mu|E,n^+\rangle$, which enter Eq. (10), were calculated using high-order Gauss-Legendre quadrature. In Fig. 3, the magnitude of the free-bound transition dipole moments is plotted as a function of the continuum energy E.

The initial state of the system is described by a normalized Gaussian wave packet of incoming scattering states

$$|\Psi(t=0)\rangle=\int dE\ b^0_{E,1}|E,1^+\rangle, \tag{26}$$

where

$$b^0_{E,1}=b_{E,1}(t_0)=(\delta_E^2\pi)^{-1/4}\exp\left(-\frac{(E-E_i)^2}{2\delta_E^2}\right). \tag{27}$$

Simulations were made for initial collision energies of $E_i=0.0$–0.03 a.u. and wave packet widths $\delta_E=10^{-4}$–10^{-3} cm^{-1}. It is evident from Fig. 3 that the bound-continuum matrix elements do not vary appreciably with kinetic energy over these widths. Therefore, we rewrite Eq. (17) as

$$F_1(t)=\Omega_{0,E_i,1}(t)\int dE\ \exp[-i\Delta_E t]b^0_{E,1} \tag{28}$$

and obtain from Eqs. (27) and (28) that

$$F_1(t)=(4\delta_E^2\pi)^{1/4}\Omega_{0,E_i,1}(t)\exp\left\{-\frac{\delta_E^2t^2}{2\hbar^2}-i\Delta_{E_i}t\right\}. \tag{29}$$

Choosing a Gaussian pulse of the form

$$\epsilon(t)=\epsilon^0\exp\left\{-\left(\frac{t-t_p}{\Delta t}\right)^2\right\}, \tag{30}$$

we can write Eq. (29) as

$$F_1(t)=\frac{(4\delta_E^2\pi)^{1/4}}{\hbar}\langle 0|\mu|E_i,1^+\rangle\epsilon^0 \times\exp\left\{-\left(\frac{t-t_p}{\Delta t}\right)^2-i\Delta_{E_i}t-\frac{\delta_E^2t^2}{2\hbar^2}\right\}. \tag{31}$$

Having computed all input matrix elements, the dynamics, embodied in Eq. (15), is solved using either a Runge-Kutta-Merson (RKM) algorithm for direct numerical integration or the exact expression of Eq. (21). Both methods give identical results, thus confirming the validity of the analytical solution. The resulting $b_0(t)$ coefficient is then used to calculate the continuum population distributions $b_{E,1}(t)$ and $b_{E,2}(t)$ according to Eq. (12).

The energy dependence of the nonradiative reaction probability is presented in Fig. 4 and the time dependence of the expansion coefficients are shown in Fig. 5. Initial collision energy for this calculation was 0.01 atomic units. From Fig. 4 it is evident that the nonradiative reaction probability at this energy is negligible. The effect of the laser pulse is to induce a near-complete ($>99\%$) population transfer from the wave packet of $|E,1^+\rangle$ states (localized to the left of the potential barrier) to a wave packet of $|E,2^+\rangle$ states (localized to the right of the barrier), while keeping the population of

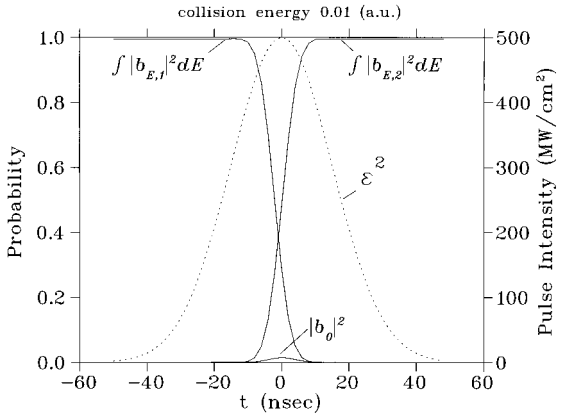

FIG. 5. Integrated populations of incoming and outgoing continuum states and the population of the $v=0$ intermediate state vs time. Dashed line is the intensity profile of the Gaussian pulse whose maximum intensity is 5×10^8 W/cm^2. The FWHM of the pulse is 30 nsec and its central frequency was chosen so that $\Delta_{E_i}=0$. The initial reactant collision energy is 0.01 a.u. and initial wave packet width is $\delta_E=10^{-3}$ cm^{-1}.

the $|0\rangle$ states to a bare minimum. In this way spontaneous emission losses are essentially eliminated.

Due to an exact scaling relation in Eq. (15), it is possible to use pulses of different duration and intensity. When the initial wave packet width, laser detuning, and pulse intensity are scaled down as

$$\delta_E \rightarrow \frac{\delta_E}{s}, \quad \Delta_{E_i} \rightarrow \frac{\Delta_{E_i}}{s}, \quad \epsilon^0 \rightarrow \frac{\epsilon^0}{\sqrt{s}},$$

and pulse duration and time are scaled up as

$$\Delta t \rightarrow \Delta t s, \quad t_p \rightarrow t_p s.$$

It follows from Eqs. (31) and (16) that under these transformations

$$F_1(t) \rightarrow \overline{F}_1(t) = \frac{F_1(t/s)}{s}, \quad \Omega_{1,2}(t) \rightarrow \overline{\Omega}_{1,2}(t) = \frac{\Omega_{1,2}(t/s)}{s},$$

and Eq. (15) becomes

$$\frac{d}{dt/s} b_0 = iF_1(t/s) - [\Omega_1(t/s) + \Omega_2(t/s)]b_0. \qquad (32)$$

We see that the scaled coefficients at time t are identical to the unscaled coefficients at times t/s. Therefore, pulse duration and intensity may be varied as long as the integrated pulse power $|\epsilon^0|^2\Delta t$ is not changed. This behavior is demonstrated in Figs. 6(a) and 6(b). A short-pulse case is illustrated in Fig. 6(a), whereas a long-pulse case, with a narrower bandwidth (longer duration) initial wave packet, is shown in Fig. 6(b). It is evident that the time evolution of the system is scaled up by a factor of 10, whereas pulse intensity is scaled down by the same factor. The advantage of long pulses is that only reactants that will collide during the laser pulse will react. Thus, longer pulses would increase the number of product molecules formed within a single pulse duration. The disadvantage is that the power requirements become increasingly more difficult to fulfill the longer the pulse, because the peak power must go down exactly as $1/\Delta t$, whereas in most practical devices the power goes down much faster with increasing pulse durations.

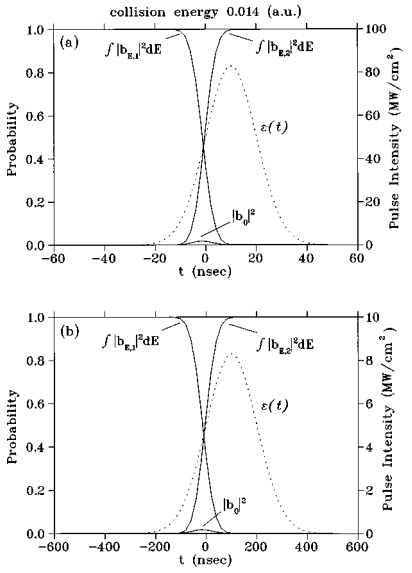

FIG. 6. Integrated populations of incoming and outgoing continuum states and the population of the $v=0$ intermediate state vs time. Dashed lines are pulse intensity profiles. The initial reactant collision energy is 0.014 a.u. (a) Initial wave packet width of $\delta_E=10^{-3}$ cm^{-1}. Pulse intensity is 83 MW/cm^2 and its FWHM is 20 nsec. (b) Initial wave packet width of $\delta_E=10^{-4}$ cm^{-1}. Pulse intensity is 8.3 MW/cm^2 and its FWHM is 200 nsec.

As mentioned above, by keeping the population of the intermediate resonance low (as is the case in Fig. 5) we effectively eliminate the spontaneous emission losses. In Fig. 7, we plot the intermediate level population as a function of t at four different pulse intensities. Radiative reaction probability for all plotted intensities is near unity. However, it is evident that the intermediate state population throughout the process decreases with increasing pulse intensity. Thus, to avoid spontaneous emission losses, high pulse intensities should be used.

Calculated reactive line shapes (i.e., the reaction probabil-

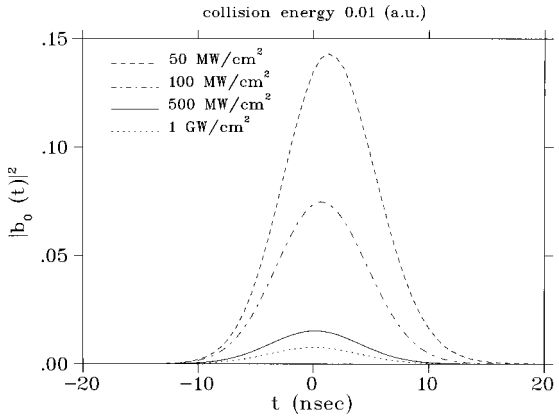

FIG. 7. Intermediate state population vs time at pulse intensities of 50 MW/cm^2, 100 MW/cm^2, 500 MW/cm^2 and 1 GW/cm^2. Pulse duration and central frequency and initial kinetic energy of the reactants are as in Fig. 5.

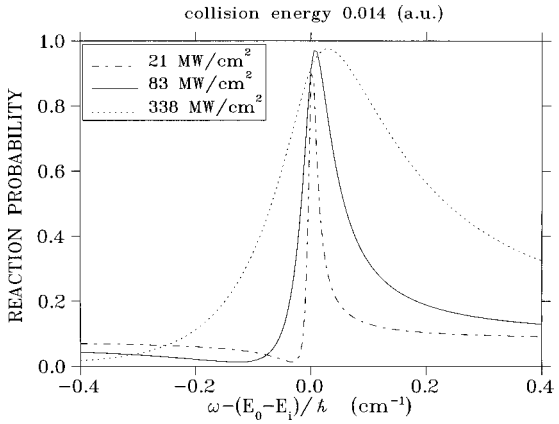

FIG. 8. Calculated reactive line shapes at 21, 83, and 338 MW/cm^2. The FWHM of the pulse is 20 nsec. Reactants collision energy is 0.014 a.u. and the initial wave packet width is $\delta_E = 10^{-3}$ cm^{-1}.

ity as a function of the pulse center frequency) at three pulse intensities are shown in Fig. 8. The initial collision energy is 0.014 a.u., i.e., slightly closer to the barrier maximum than before. According to Fig. 4, the nonradiative reaction probability is now about 9%. This causes the line shapes to assume an asymmetric form due to the interference between the nonradiative tunneling pathway and the laser catalyzed pathway. We see that the reaction probability is enhanced for a positive (blue) detuning and suppressed for a negative (red) detuning. This result is similar to the findings in the cw case, accept that the power requirements can be easily met and spontaneous emission is essentially nonexistent.

The effects noted above are absent in the weak field limit, namely when the field is too weak the maximal reaction probability is less than unity. As shown in Fig. 9, before reaching saturation, marked by unit reaction probability at the right frequency, the reaction probability increases monotonically with increasing laser intensity. This is in contrast with the cw results [15], where the sole effect of the reduction in laser power is to narrow down the asymmetric line shapes of Fig. 8 while leaving one point of perfect transmission at the center of the line.

The existence of a point where the reaction probability assumes the value of 1 is best understood by adopting the

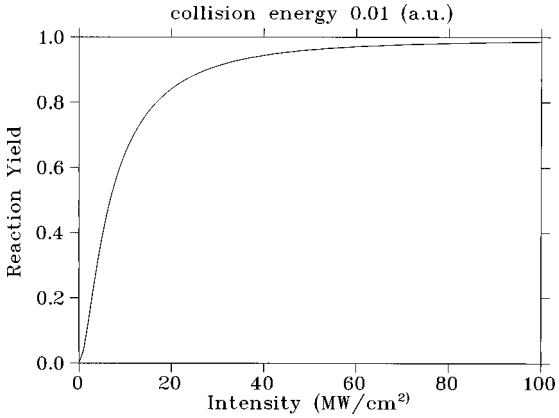

FIG. 9. Reactive probability vs pulse intensity for a fixed wave packet spectral width. Pulse width and central frequency are as in Fig. 5.

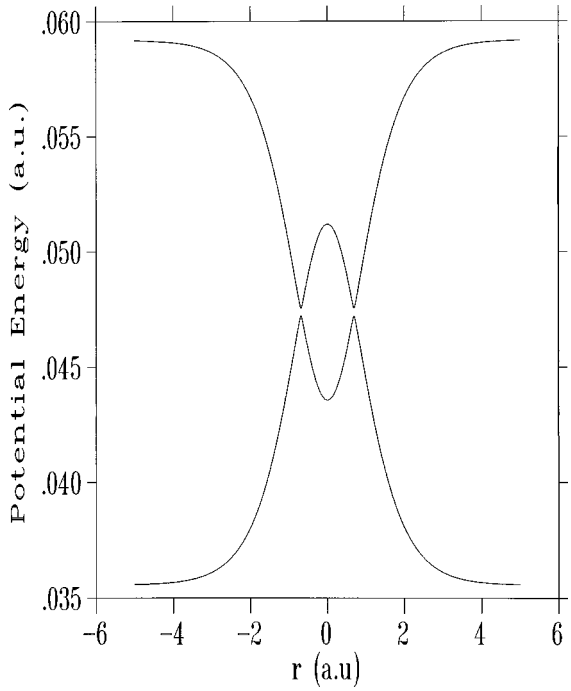

FIG. 10. Dressed state potentials for the laser catalysis process at maximum pulse intensity. Initial kinetic energy is 0.01 a.u.

''(photon) dressed states'' picture. When the 2×2 dressed-potential matrix composed of the (diagonal) dressed potentials and the (off-diagonal) field-dipole coupling terms is diagonalized, the two field-matter eigenvalues shown in Fig. 10 result. As demonstrated in Fig. 10, the ground field-matter eigenvalue assumes the shape of a double-barrier potential and the excited eigenvalue—the shape of a double-well potential. The separation between these eigenvalues gets larger as the coupling field strength is increased.

In the adiabatic approximation, particles starting out in the remote past in the ground state remain on the lowest eigenvalue at all times. These particles experience resonance scattering by a double-barrier potential, admitting tunneling probability of unity, irrespective of the details of the potential [34–40], when the incident energy is near a quasibound state of the well within the barriers. Similar phenomena have been noted for semiconductor devices [34–40], in the context of the Ramsauer-Townsend effect [41] and for Fabry-Pérot interferometers [42]. In addition, field-induced transparency, observed when a high-frequency field acts on a single barrier, was explained as a result of the emergence of an average field-dressed double-barrier potential [43].

The point of tunneling suppression (i.e., when the tunneling probability of Fig. 8 assumes the value of 0) appears, in the dressed-states picture, as a result of the breakdown of the adiabatic approximation: At the energy of tunneling suppression, the flux leaking to the excited double-well eigenvalue interferes destructively with the flux remaining on the low double-barrier potential.

ACKNOWLEDGMENTS

This work was supported by the James Franck program of the Minerva Foundation, by Bram and Bluma Appel, Toronto, and by a grant from the Israel Science Foundation.

APPENDIX: THE WAVE FUNCTIONS OF THE ECKART POTENTIAL

The eigenfunctions of a Hamiltonian with an Eckart potential [Eq. (22)] are given in terms of hypergeometric functions [29,30],

$$F(a,b,c,y)=1+\frac{ab}{1\times c}\,y+1\,\frac{a(a+1)b(b+1)}{1\times 2\times c(c+1)}\,y^2+\cdots, \tag{A1}$$

in terms of which the outgoing scattering wave functions are given as

$$\langle x|E,1^+\rangle=T_1(1-\xi)^{i\beta}\left(\frac{\xi}{\xi-1}\right)^{i\alpha}F\left\{\tfrac{1}{2}+i(\alpha-\beta+\delta),\tfrac{1}{2}+i(\alpha-\beta-\delta),1-2i\beta,\ \frac{1}{1-\xi}\right\}, \tag{A2}$$

where

$$\alpha=\sqrt{E/4C}=\frac{l}{2\pi}\,k_1,\quad \beta=\sqrt{(E-A)/4C}=\frac{l}{2\pi}\,k_2,\quad \delta=\sqrt{(B-C)/4C};\quad C=\frac{h^2}{8ml^2}. \tag{A3}$$

In Eq. (A2) we have corrected a sign error in the expression for the b parameter that appeared at Ref. [29] and persisted in Ref. [30]. Since $F(a,b,c,0)=1$, it is evident that the asymptotic condition for large positive x (large ξ) given in Eq. (1b) is fulfilled,

$$\lim_{x\to\infty}\langle x|E,1^+\rangle=T_1(-\xi)^{i\beta}=T_1\exp(ik_2x). \tag{A4}$$

To determine asymptotic behavior for large negative x (small ξ), we use the linear transformation formula [33]

$$F(a,b,c,z)=\frac{\Gamma(c)\Gamma(c-a-b)}{\Gamma(c-a)\Gamma(c-b)}\,F(a,b,a+b-c+1,1-z)+\frac{\Gamma(c)\Gamma(a+b-c)}{\Gamma(a)\Gamma(b)}\,(1-z)^{c-a-b}F(c-a,c-b,c-a-b+1,1-z). \tag{A5}$$

Application of identity (A5) to Eq. (A2) results in an expression for the incoming scattering states in terms of two series that converge for small ξ values,

$$\begin{aligned}\langle x|E,1^+\rangle=&\,c_1\left(\frac{\xi}{\xi-1}\right)^{i\alpha}(1-\xi)^{i\beta}F\left\{\frac{1}{2}+i(\alpha-\beta+\delta),\ \frac{1}{2}+i(\alpha-\beta-\delta),1+2i\alpha,\ \frac{\xi}{\xi-1}\right\}\\&+c_2\left(\frac{\xi}{\xi-1}\right)^{-i\alpha}(1-\xi)^{i\beta}F\left\{\frac{1}{2}+i(-\alpha-\beta-\delta),\ \frac{1}{2}+i(-\alpha-\beta+\delta),1-2i\alpha,\ \frac{\xi}{\xi-1}\right\},\end{aligned} \tag{A6}$$

where

$$c_1=T_1\,\frac{\Gamma(1-2i\beta)\Gamma(-2i\alpha)}{\Gamma[\tfrac{1}{2}+i(-\alpha-\beta-\delta)]\Gamma[\tfrac{1}{2}+i(-\alpha-\beta+\delta)]} \tag{A7}$$

and

$$c_2=T_1\,\frac{\Gamma(1-2i\beta)\Gamma(+2i\alpha)}{\Gamma[\tfrac{1}{2}+i(\alpha-\beta-\delta)]\Gamma[\tfrac{1}{2}+i(\alpha-\beta+\delta)]}. \tag{A8}$$

For large negative values of x (small ξ) we have

$$\lim_{x\to-\infty}\langle x|E,1^+\rangle=c_1(-\xi)^{i\alpha}+c_2(-\xi)^{-i\alpha}=c_1\exp(ik_1x)+c_2\exp(-ik_1x). \tag{A9}$$

By comparison with Eq. (1a),

$$c_1=\left(\frac{m}{k_1h}\right)^{1/2},\quad c_2=R_1, \tag{A10}$$

and we can determine the constants T_1 and R_1 to be

$$T_1=\frac{\Gamma[\tfrac{1}{2}+i(-\alpha-\beta-\delta)]\Gamma[\tfrac{1}{2}+i(-\alpha-\beta+\delta)]}{\Gamma(1-2i\beta)\Gamma(-2i\alpha)}\left(\frac{m}{k_1h}\right)^{1/2}, \tag{A11}$$

$$R_1=\frac{\Gamma(+2i\alpha)\Gamma[\frac{1}{2}+i(-\alpha-\beta-\delta)]\Gamma[\frac{1}{2}+i(-\alpha-\beta+\delta)]}{\Gamma(-2i\alpha)\Gamma[\frac{1}{2}+i(\alpha-\beta-\delta)]\Gamma[\frac{1}{2}+i(\alpha-\beta+\delta)]}\left(\frac{m}{k_1h}\right)^{1/2}. \tag{A12}$$

The nonradiative reflection coefficient is thus given as

$$\sigma(R_1)=\frac{k_1h}{m}|R_1|^2=\left|\frac{\Gamma(\frac{1}{2}+i(-\alpha-\beta-\delta))\Gamma(\frac{1}{2}+i(-\alpha-\beta+\delta))}{\Gamma(\frac{1}{2}+i(\alpha-\beta-\delta))\Gamma(\frac{1}{2}+i(\alpha-\beta+\delta))}\right|^2 \tag{A13}$$

and the nonradiative transmission coefficient is

$$\sigma(T_1)=\frac{k_2h}{m}|T_1|^2=\frac{\beta}{\alpha}\left|\frac{\Gamma[\frac{1}{2}+i(-\alpha-\beta-\delta)]\Gamma[\frac{1}{2}+i(-\alpha-\beta+\delta)]}{\Gamma(1-2i\beta)\Gamma(-2i\alpha)}\right|^2. \tag{A14}$$

The intermediate state was taken to be one of the vibrational states of an inverse Eckart given by Eq. (23). Bound-state energies for the time-independent Schrödinger equation with this potential are given as

$$E_n=\mathcal{E}-\frac{A}{2}-[\delta'-(n+\tfrac{1}{2})]^2C-\left[\frac{1}{4[\delta'-(n+\frac{1}{2})]}\right]^2\frac{A^2}{C}, \tag{A15}$$

where $\delta'=\sqrt{(B+C)/4C}$, $C=h^2/8ml^2$, and

$$n=0,1,2,\ldots,<\delta'-\tfrac{1}{2}-\sqrt{A/4C}. \tag{A16}$$

Corresponding eigenfunctions are given as

$$\psi_n(x)=N(1-\xi)^{-\beta_n}\left(\frac{\xi}{\xi-1}\right)^{-\alpha_n}F\left\{-n,2\delta'-n,1+2\beta_n,\frac{1}{1-\xi}\right\}, \tag{A17}$$

where

$$\alpha_n=\left(\frac{\mathcal{E}-E_n}{4C}\right)^{1/2};\quad \beta_n=\left(\frac{\mathcal{E}-E_n-A}{4C}\right)^{1/2}. \tag{A18}$$

[1] For reviews, see *Molecules in Laser Fields*, edited by A. D. Bandrauk (Marcel Dekker, New York, 1994).

[2] M. V. Fedorov, O. V. Kudrevatova, V. P. Makarov, and A. A. Samokhin, Opt. Commun. **13**, 299 (1975).

[3] N. M. Kroll and K. M. Watson, Phys. Rev. A **8**, 804 (1973); **13**, 1018 (1976).

[4] J. I. Gerstein and M. H. Mittleman, J. Phys. B **9**, 383 (1976).

[5] J. M. Yuan, T. F. George, and F. J. McLafferty, Chem. Phys. Lett. **40**, 163 (1976); J. M. Yuan, J. R. Laing, and T. F. George, J. Chem. Phys. **66**, 1107 (1977); T. F. George, J. M. Yuan, and I. H. Zimmermann, Faraday Discuss. Chem. Soc. **62**, 246 (1977); P. L. DeVries and T. F. George, *ibid.* **67**, 129 (1979); T. F. George, J. Phys. Chem. **86**, 10 (1982).

[6] A. M. F. Lau and C. K. Rhodes, Phys. Rev. A **16**, 2392 (1977); A. M. F. Lau, *ibid.* **13**, 139 (1976); **25**, 363 (1981).

[7] V. S. Dubov, L. I. Gudzenko, L. V. Gurvich, and S. I. Iakovlenko, Chem. Phys. Lett. **45**, 351 (1977).

[8] A. D. Bandrauk and M. L. Sink, Chem. Phys. Lett. **57**, 569 (1978); J. Chem. Phys. **74**, 1110 (1981).

[9] A. E. Orel and W. H. Miller, Chem. Phys. Lett. **57**, 362 (1978); **70**, 4393 (1979); **73**, 241 (1980).

[10] J. C. Light and A. Altenberger-Siczek, J. Chem. Phys. **70**, 4108 (1979).

[11] K. C. Kulander and A. E. Orel, J. Chem. Phys. **74**, 6529 (1981).

[12] H. J. Foth, J. C. Polanyi, and H. H. Telle, J. Phys. Chem. **86**, 5027 (1982).

[13] T. Ho, C. Laughlin, and S. I. Chu, Phys. Rev. A **32**, 122 (1985).

[14] M. Shapiro and Y. Zeiri, J. Chem. Phys. **85**, 6449 (1986).

[15] T. Seideman and M. Shapiro, J. Chem. Phys. **88**, 5525 (1988); **92**, 2328 (1990); **94**, 7910 (1991).

[16] T. Seideman, J. L. Krause, and M. Shapiro, Chem. Phys. Lett. **173**, 169 (1990); Faraday Discuss. Chem. Soc. **91**, 271 (1991).

[17] A. Zavriyev, P. H. Bucksbaum, H. G. Muller, and D. W. Schumacher, Phys. Rev. A **42**, 5500 (1990).

[18] A. Guisti-Suzor and F. H. Mies, Phys. Rev. Lett. **68**, 3869 (1992).

[19] G. Yao and S.-I. Chu, Chem. Phys. Lett. **197**, 413 (1992).

[20] E. E. Aubanel and A. D. Bandrauk, Chem. Phys. Lett. **197**, 419 (1992); A. D. Bandrauk, E. E. Aubanel, and J. M. Gauthier, Laser Phys. **3**, 381 (1993).

[21] D. R. Matusek, M. Yu. Ivanov, and J. S. Wright, Chem. Phys. Lett. **258**, 255 (1996).

[22] U. Fano, Phys. Rev. **124**, 1866 (1961).

[23] D. J. Tannor and S. A. Rice, J. Chem. Phys. **83**, 5013 (1985);

D. J. Tannor, R. Kosloff, and S. A. Rice, *ibid.* **85**, 5805 (1986); D. J. Tannor, in *Molecules in Laser Fields* (Ref. [1]), p. 403.
[24] T. Seideman, M. Shapiro, and P. Brumer, J. Chem. Phys. **90**, 7132 (1989); I. Levy, M. Shapiro, and P. Brumer, *ibid.* **93**, 2493 (1990).
[25] M. Shapiro, J. Chem. Phys. **101**, 3844 (1994).
[26] E. Frishman and M. Shapiro, Phys. Rev. A **54**, 3310 (1996).
[27] A. Vardi and M. Shapiro, J. Chem. Phys. **104**, 5490 (1996).
[28] A. Vardi, D. Abrashkevich, E. Frishman, and M. Shapiro, J. Chem. Phys. **107**, 6166 (1997).
[29] C. Eckart, Phys. Rev. **35**, 1303 (1930).
[30] H. Eyring, J. Walter, and G. E. Kimball, *Quantum Chemistry* (Wiley, New York, 1944).
[31] B. Liu, J. Chem. Phys. **58**, 1925 (1973).
[32] D. G. Truhlar and C. J. Horowitz, J. Chem. Phys. **68**, 2466 (1978).
[33] *Handbook of Mathematical Functions*, edited by M. Abramowitz and I. A. Stegun (Dover, New York, 1965).
[34] R. Tsu and L. Esaki, Appl. Phys. Lett. **22**, 562 (1973).
[35] L. L. Chang, L. Esaki, and R. Tsu, Appl. Phys. Lett. **24**, 593 (1974).
[36] S. C. Kan and A. Yariv, J. Appl. Phys. **67**, 1957 (1990).
[37] A. Sa'ar, S. C. Kan, and A. Yariv, J. Appl. Phys. **67**, 3892 (1990).
[38] H. Yamamoto, Y. Kanie, M. Arakawa, and K. Taniguchi, Appl. Phys. A: Solids Surf. **50**, 577 (1990).
[39] W. Cai, T. F. Zheng, P. Hu, M. Lax, K. Shun, and R. Alfano, Phys. Rev. Lett. **65**, 104 (1990).
[40] K. A. Chao, M. Willander, and Yu. M. Galperin, Phys. Scr. **T54**, 119 (1994).
[41] J. R. Taylor, *Scattering Theory* (Wiley, New York, 1972), Chap. 11.
[42] A. Yariv, *Optical Electronics*, 4th ed. (Saunders College, Philadelphia, 1991).
[43] I. Vorobeichik, R. Lefebvre, and N. Moiseyev, Europhys. Lett. **41**, 111 (1998).